



Trans. Nonferrous Met. Soc. China 30(2020) 944-957

Transactions of Nonferrous Metals Society of China

www.tnmsc.cn



Biological, antibacterial activities and electrochemical behavior of borided commercially pure titanium in BSA-containing PBS

Adib EBRAHIMI, Hamid ESFAHANI, Omid IMANTALAB, Arash FATTAH-ALHOSSEINI

Department of Materials Engineering, Bu-Ali Sina University, Hamedan 65178-38695, Iran

Received 10 June 2019; accepted 18 February 2020

Abstract: The effects of boride coating on the bioactivity, antibacterial activity, and electrochemical behavior of commercially pure titanium (CP-Ti) in phosphate buffer solution (PBS) with bovine serum albumin (BSA) were studied. The grazing incidence X-ray diffraction (GIXRD) pattern confirmed the formation of a TiB/TiB₂ coating via boriding process. Scanning electron microscopy (SEM) observation indicated that the TiB₂ cross-linked particles covered the TiB whiskers. Water contact angle measurements revealed that boriding led to the formation of a surface with intermediate water affinity. Potentiodynamic polarization (PDP) assays demonstrated that the TiB/TiB₂ coating had acceptable passivation behavior in BSA-containing PBS. Electrochemical impedance spectroscopy (EIS) measurements revealed that the passivation behavior of the CP-Ti and the borided samples was improved by increasing exposure time. Based on the Mott–Schottky (M–S) tests, it was realized that the charge carriers of passive films of both samples decreased with increasing exposure time in BSA-containing PBS. The bioactivity test results in a simulated body fluid showed that the TiB/TiB₂ coating switched the CP-Ti from bioinert to bioactive material. Finally, the antibacterial activity test of the TiB/TiB₂ coating against *Escherichia coli* and *Staphylococcus aureus* indicated 99% antibacterial activity.

Key words: electrochemical behavior; boriding; BSA-containing PBS; passive film; titanium boride

1 Introduction

Commercially pure titanium (CP-Ti) is well known in the area of biomedical applications due to the high specific strength value and corrosion resistance issued by the titanium dioxide (TiO₂) passive film. However, its development for implant applications needs serious modifications, especially on the surface [1]. Surface modification is required not only for improvement of physical and mechanical properties but also for enhancement of biomimetic behavior [2]. The destruction of the TiO₂ passive film is a major problem during implantation. Weak tribology and bioinert behavior are other challenges to implantation [3]. Therefore, the novelty of this study is the utilization of surface modification of titanium through boriding to

achieve the implant requirements in terms of biological and antibacterial activities. Furthermore, the boride layers protect the titanium against the body environment due to the stable passive film formation, high wear resistance and super high adhesion to the titanium surface [4]. Among the boriding methods [5–7], the pack cementation method is a simple, cost-benefit and practical method to create the diversity of TiB, Ti₃B₄ and TiB₂ intermetallic phases on the titanium surface [8]. Furthermore, titanium borides have excellent adhesion and good coincidence of the thermal expansion coefficient with the Ti substrate [9,10].

Numerous reports are available regarding the electrochemical properties of titanium. In our previous work, we studied the electrochemical behavior of the TiB/TiB₂ coating on the Ti substrate

in some simulated body fluid solutions with respect to the primary essential requirements for any biomaterial [4,9]. We found that boriding at 900 °C (at which TiB/TiB₂ coating formed on the CP-Ti) resulted in the most suitable electrochemical behavior in both Ringer's and Hanks' solutions. In this study, the electrochemical assays of the TiB/TiB₂ coating were conducted in BSAcontaining PBS because aminoacids in the protein structure have a significant role in biomolecular adsorption and bioactive interactions during bone tissue regeneration [11]. Furthermore, the serum proteins in blood may degrade the titanium surrounded with body fluids [12]. KORNYUSHOVA et al [13] found that the adsorption of proteins on the Ti electrode surface followed different patterns due to the difference in adsorption modes among aminoacids. It has been reported that BSA proteins can be adsorbed on the titanium surface during the electrochemical assays, resulting in the kinetics of repassivation [12].

Based on the literature review, numerous studies have focused on the enhancement of the bioactivity of titanium via several kinds of surface modifications, but the influence of boriding on the element's bioactivity has rarely been investigated. It has been reported that the TiB₂ coating may promote bone-like apatite formation on the TiB₂/hydroxyapatite coating [2]. Despite its high resistance to corrosion, Ti is susceptible to bacterial infection and consequent biofilm formation after implantation [14]. Such biofilms cannot be destroyed using antibiotics and prevent bone regeneration [15,16]. Therefore, it is essential for the Ti implant to have an appropriate antibacterial effect.

The present work focused on the boriding of CP-Ti via the pack cementation method to obtain a TiB/TiB₂ coating on the CP-Ti surface. The responses of pure and borided titanium to BSA-containing PBS were investigated via electrochemical assays including the open circuit potential (OCP), potentiodynamic polarization (PDP), electrochemical impedance spectroscopy (EIS), and Mott–Schottky (M–S) assays. The bioactivity of the TiB/TiB₂ coating was evaluated in the simulated body fluid (SBF). Finally, the antibacterial effect of the mentioned coating was studied against *Escherichia coli* (*E. coli*) and *Staphylococcus aureus* (*S. aureus*).

2 Experimental

2.1 Sample processing

The CP-Ti grade 2 specimen (Ti: balance, Fe: 0.05, O: 0.19, N: 0.004, H: 0.0009, all in at.%) was polished with 2000 grit sandpaper and cleaned carefully prior to the boriding process via immersion in a specific solution (10 mL HNO₃, 1 mL HF, and 89 mL H₂O). The boriding process of the sample was performed via the pack cementation method. The powder composition of the process was 50 wt.% B powder (Merck, 112070), 35 wt.% activated charcoal (Merck, 102184) and 15 wt.% NaCO₃ (Merck, 106392). The boriding process was proceeded at 900 °C for 3 h under atmospheric conditions. Prior to further investigations, the obtained sample (called TB900) was polished and etched using the previously mentioned solution (10 mL HNO₃, 1 mL HF, and 89 mL H₂O).

2.2 Structural and morphological characterization

The grazing incidence XRD pattern of the borided was provided by Philips Xpert-MPD using Cu K_a radiation (λ =0.1540 nm) with an incidence angle of 1°. The microstructures of pure and borided CP-Ti after bioactivity tests were studied by scanning electron microscopy (SEM; FEI ESEM Quanta 200). ImageJ software (1.38X,NIH-USA) was used for further microstructural investigations. The wetting ability of the bare and borided CP-Ti surfaces was evaluated by measuring the water contact angle (WCA). Deionized water was dropped onto the sample surface before the variation of the WCA was monitored over 30 s. To ensure reproducibility, all measurements were made thrice and the average was reported.

2.3 Electrochemical characterization

The electrochemical assays were performed using a galvanostat/potentiostat set (μAutolab Type III/FRA2) coupled with a personal computer. A PBS with pH adjusted to 7.4 (20 g/L Na₂HPO₄ + 1 g/L Na₃PO₄) was used as the test solution at body temperature (37 °C). The assays were performed in 250 mL of quiescent PBS solution containing 400 mg/L of BSA (Sigma Aldrich, 9048-46-8) using a conventional glass three-electrode flat cell. The CP-Ti (bare Ti) or borided (TB900) sample, a

platinum foil, and a saturated silver chloride electrode (Ag/AgCl, KCl (sat)) were used as the working electrode, counter electrode, and reference electrode, respectively. Prior to each electrochemical assay, the working electrode was rinsed with distilled water, subjected to ultrasonic cleaning for 10 min, and dried with a stream of cold air. For the PDP test, the working electrode was immersed in the test solution for 120 h. For this analysis, the sweep scan rate was 1 mV/s, and the potential was scanned and registered in the cathode to anode direction. The starting potential was -0.250 V (vs OCP), and the potential terminated when the potential of the TB900 sample reached the breakdown potential of the passive layer. The EIS data acquisition was carried out under OCP conditions potentiostatically by applying an AC frequency range from 10⁵ to 10⁻³ Hz with an excitation potential (RMS voltage) of 10 mV. The analyses, such as Kramers-Kronig transformation (KKT) and fitting of the EIS data were carried out using Nova software. Meanwhile, reproducibility of the obtained electrochemical results was ensured through five repetitions of each test; the average value of each electrochemical parameter was reported. For the M-S technique, the step rate was 25 mV with a potential scan range from 0.6 to -0.8 V (vs Ag/AgCl). All the M-S assays were done at a fixed frequency of 1×10⁴ Hz using an excitation potential of 10 mV in the cathodic direction.

2.4 Biological characterization

The bioactivity test of the CP-Ti and TB900 samples was performed based on the Kokubo procedure [17]. In this order, the 1 cm × 1 cm specimens were soaked in the SBF solution at biological temperature (37 °C) for several periods of time (1, 3, 14, and 21 d). The surface of each sample was washed using deionized water and then dried at 80 °C prior to the morphological study.

In accordance to the ASTM G21–1996, the antibacterial activity testing of the CP-Ti and TB900 samples was performed in a solution containing two kinds of bacterial species. These species included *S. aureus* (ATCC 25923) and *E. coli* (ATCC 25922), which represent grampositive and gram-negative bacteria, respectively. The bacteria were prepared and adjusted by spectrophotometry. All samples were sterilized and

then placed in sterilized tubes containing certain amounts of each bacterial species (1×10³ cfu/mL) based on the spot induction method. The samples were then incubated in Mueller–Hinton agar (Merck, KGaA) for 24 h at 37 °C in order to evaluate their antibacterial activity.

3 Results and discussion

3.1 Characterization of boride layers

To understand the formation of the boride phases at the top of the CP-Ti surface, the GIXRD technique was applied. Figure 1 shows the GIXRD pattern of the borided sample. Based on the No. 01-073-2148 standard card of the Joint Committee on Powder Diffraction Standards (JCPDS), TiB was recognized as the main component of the boride coating. It was also found that TiB₂ (JCPDS No. 01-075-0967 standard card) existed as the second phase alongside the TiB. Although Ti₃B₄ is another common phase in the Ti-B system, the corresponding peaks were not detected. Moreover, no peaks indicative of a TiO₂ phase were found in the GIXRD pattern. This meant that the boriding process was performed well. According to the results of phase identification, it can be said that the TiB and TiB2 were the main components of the boride coating. The diffusion coefficient of B into TiB and TiB2 is intensified with an increase in the temperature of boriding based on the studies of MURRAY et al [18]. It should be mentioned that the diffusion coefficient of B into TiB and TiB₂ is 10^3-10^4 times higher than that of Ti in the mentioned phases [18]. Hence, more B atoms could diffuse into the Ti substrate due to the faster diffusion of B atoms in [010] direction, thereby facilitating the formation of TiB whiskers [8,19].

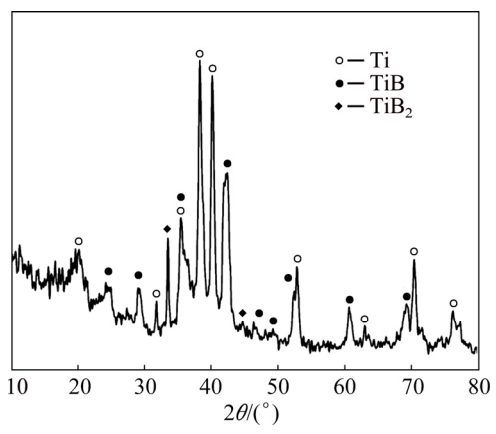


Fig. 1 GIXRD pattern of borided sample

Figure 2(a) shows SEM image of the top surface of CP-Ti after boriding at 900 °C for 3 h. As seen, the boriding process caused the formation of cross-linked particles with an average size of (1.6 ± 0.3) µm on top of the CP-Ti surface. Based on our previous work, these particles can be attributed to the TiB₂ phase [4,9]. The cross-section view in Fig. 2(b) indicates the deep penetration of the TiB whiskers well into the Ti substrate under the top TiB₂ layer. The average thickness of the top TiB₂ layer on the CP-Ti and the length of the TiB whiskers were (1.2 ± 0.2) µm and (3.9 ± 0.2) µm, respectively. The preferential orientation of the TiB whiskers and the hard nature of the TiB2 top layer give rise to a super-adhesive coating suitable for load-bearing implants [9].

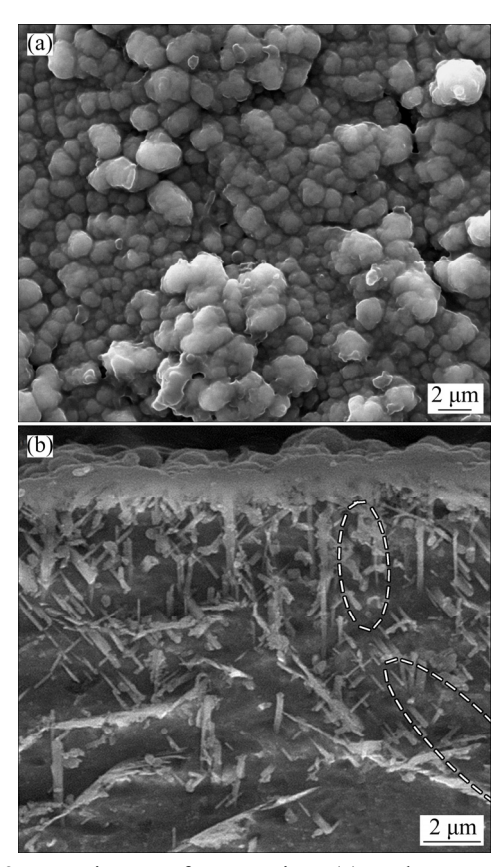


Fig. 2 SEM images for top view (a) and cross-section surface (b) of CP-Ti after boriding at 900 °C for 3 h

Wetting ability plays a significant role in protein adsorption [20]. Therefore, the wetting ability of the bare CP-Ti and TB900 samples was evaluated based on the WCA measurements. Figure 3(a) presents the variation of WCA on the surface of the mentioned samples during the first 30 s of contact. The WCA at first contact was 54.5° (hydrophilic) on the CP-Ti, while it was 82.5° (near

hydrophobic behavior) on the TB900 [21]. Figures 3(b) and (c) show the corresponding images of the water droplets at first contact on the CP-Ti and TB900 surfaces, respectively. The formation of TiB/TiB₂ on the surface of Ti decreased the wetting ability of CP-Ti due to the development of Ti-B bonds and the generation of microtopography by the cross-linked TiB₂ particles at the top of the surface. A decreasing trend of WCA was observed for both samples; the WCA after 30 s was 38° and 63.5° on the CP-Ti and TB900 surfaces, respectively. It is worth mentioning that the wetting ability of a surface with intermediate water affinity (in-between hydrophilic and hydrophobic) is favored for the adhesion of cells or proteins [3]. Therefore, it can be elucidated that boriding CP-Ti accelerates protein adsorption and consequent cellular responses [22].

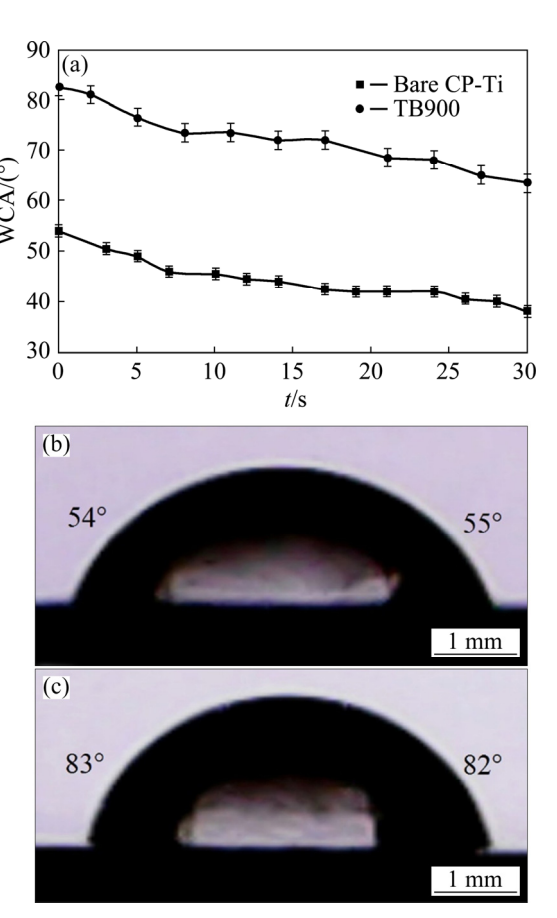


Fig. 3 Variation of WCA on bare CP-Ti and TB900 samples during 30 s (a), and images of water droplet at first contact on bare CP-Ti (b) and TB900 (c) surfaces

3.2 Electrochemical behavior

3.2.1 Potentiodynamic polarization

Figure 4 illustrates the PDP curves of the bare CP-Ti and TB900 samples in quiescent PBS

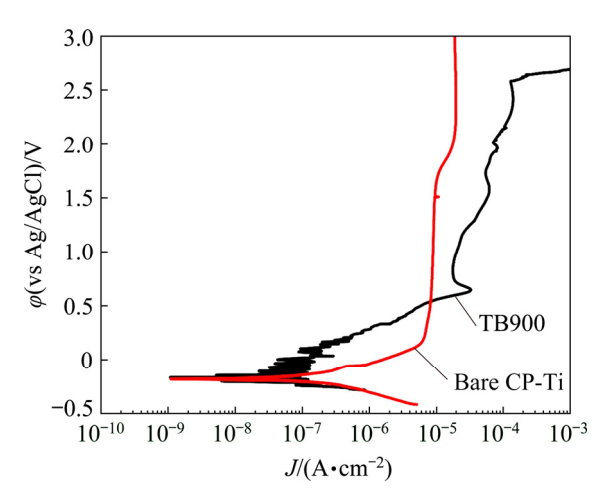


Fig. 4 PDP curves of bare CP-Ti and TB900 samples after 120 h of stabilization in PBS solution with 400 mg/L BSA

solution containing 400 mg/L of BSA. Similar PDP curves were reported for bare and borided CP-Ti samples in Ringer's and Hanks' balanced salt solutions [4,9]. Although both the bare CP-Ti and TB900 samples indicated typical passive behavior in the studied solutions, there were distinguishable differences between the two samples. Specifically, the bare CP-Ti sample had a broader passive domain compared to the TB900 sample. The passive current density of the bare CP-Ti was lower than that of the TB900 in the studied passive region. Generally, a smaller value of the passive current density represents that the passive layer forms more easily on the surface [23]. Moreover, the breakdown potential (φ_{bp}) of the passive layer is a criterion used to evaluate the passive layer susceptibility to deterioration by halide ions. Comparatively, a greater φ_{bp} value indicates the development of a more stable passive layer on the metal surface [24]. Based on published papers [4,25], the φ_{bp} of the borided CP-Ti samples in Ringer's solution at high potentials during the PDP measurements could be attributed to the localized corrosion sites. According to Fig. 4, the φ_{bp} of the TB900 sample was lower than that of the CP-Ti sample. Also, the φ_{bp} value for the TB900 sample was above 0.592 V (vs Ag/AgCl). As a result, the TB900 sample can be considered as a bioimplant material because of the in-vivo potential range of CP-Ti as well as its alloys, which ranges from 0.495 V (vs Ag/AgCl) to 0.592 V (vs Ag/AgCl) [25-27]. Table 1 lists some electrochemical parameters obtained from the PDP curves (Fig. 4) such as the corrosion current density

 (J_{corr}) , the corrosion potential (φ_{corr}) , and the breakdown potential (φ_{bp}) . According to Table 1, the corrosion current density of the TB900 sample was greater than that of the bare CP-Ti sample.

Table 1 Electrochemical parameters obtained from PDP plots of bare CP-Ti and TB900 samples in PBS solution containing 400 mg/L BSA

Sample	$\varphi_{\rm corr}$ (vs Ag/AgCl)/	$J_{ m corr}$	$\varphi_{\rm bp}$ (vs Ag/AgCl)/
	mV	$(\mu A \cdot cm^{-2})$	mV
Bare	-179	10.6	>3000
CP-Ti	-179	10.0	~3000
TB900	-164	10.07	2591

3.2.2 EIS data

technique was employed The EIS elucidating further information concerning passivation behavior of the bare CP-Ti and TB900 samples in PBS solution containing 400 mg/L of BSA as a function of immersion time [4,28–30]. The EIS results of the studied samples in different formats (i.e., Nyquist, Bode and Bode-phase plots) recorded after different immersion time are illustrated in Fig. 5. As seen, for each sample, these formats maintained general shape throughout the investigated immersion time of 1 to 120 h, representing that no changes in electrochemical mechanisms occurred. Similarly, the Nyquist and Bode plots have also been reported for bare and borided CP-Ti samples immersed in both Ringer's and Hanks' solutions [4,9].

Based the plot in the Nyquist format shown in Figs. 5(a) and (c), augmentations of the semicircles of both samples were clearly seen with increasing immersion time. Normally, a larger diameter (or radius) in the Nyquist curve verified the greater electrochemical corrosion resistance of a sample [4]. According to the plot in the Bode format shown in Figs. 5(b) and (d), it is clearly distinguishable that the values of total impedance in the middle to low frequency range were augmented with increasing exposure time across both samples. According to this plot, the maximum phase angles were less than -90°. Therefore, a deviation from ideal capacitive behavior was apparent for both samples [9]. Moreover, the vestige of two capacitance arcs was seen for both the bare CP-Ti and TB900 samples. It is worth mentioning that non-ideal capacitance behavior is recognizable from an incomplete semicircle in a Nyquist curve and a straight line

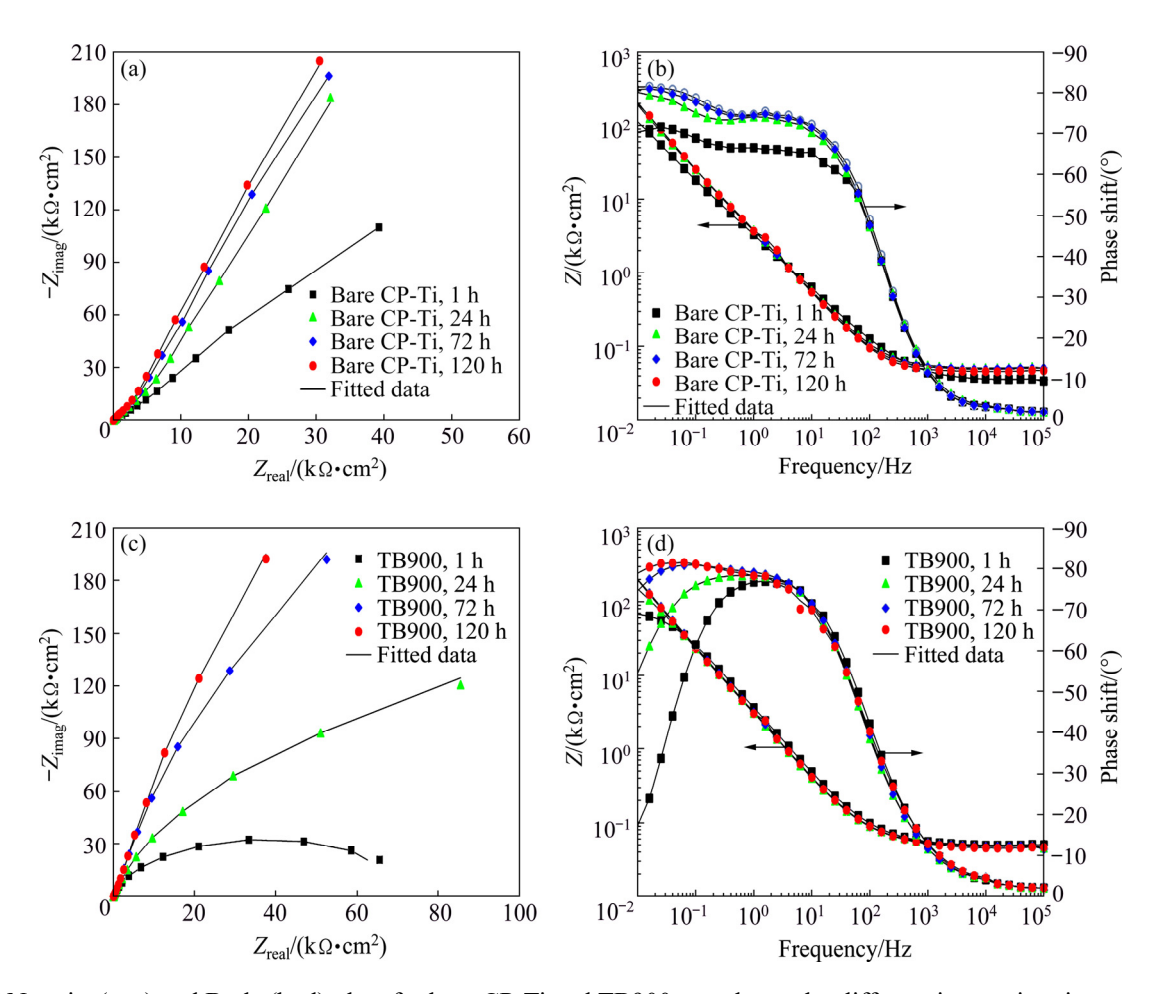


Fig. 5 Nyquist (a, c) and Bode (b, d) plots for bare CP-Ti and TB900 samples under different immersion time

with a slope of close to -1 in a Bode-phase curve [4,9]. The presence of the constant phase elements (CPEs) in the proposed electrical equivalent circuits (EECs) in lieu of the Warburg impedance (W) and pure capacitance (C) elements is a general rule for obtaining the best fit between experimental and theoretical information [29].

The emergence of CPE behavior could be ascribed to many well-known factors such as the preferential active sites (i.e., impurities and grain boundaries), existence of pores in the surface oxide films, and different types of surface heterogeneities on the working electrodes including scratches, adsorption of ions, roughness, and the impact of resistive variations that pertain to the covering films [31–35]. We measured the roughness (R_a) of the bare CP-Ti and TB900 surfaces, and it was found that the R_a parameter increased from 0.257 to 0.732 µm in the longitudinal mode and from 0.233 to 0.503 µm in the transversal mode after boriding. This meant that the heterogeneous surface of TB900 resulted in the CPE behavior. As seen in the

Bode and Bode-phase plots of both the bare CP-Ti and TB900 samples (Fig. 5), the values of the absolute impedance and phase angles at high frequencies (higher than 100 Hz) were almost constant and independent of frequency, which demonstrated pure resistive behavior (R). This behavior was attributed to the solution resistance between the reference and working electrodes. In this work, the Kramers-Kroning transformation (KKT) of the imaginary and real parts of the impedance was examined as a simple way for studying the limitations of the linear system theory (i.e., stability, causality and linearity) in order to investigate the validation of the EIS results. If any of these three limitations are not achieved, the interpretation of the EIS results may be delusive [36]. The niceties of KKT have been presented in Refs. [37,38]. The comparison between the KKT and the experimental EIS data for the bare CP-Ti and TB900 samples after 1 h of exposure to the studied solution is illustrated in Fig. 6. Clearly, correspondence between the experimental data and

the corresponding KKT ratifies the conformity of the studied system with the conditions of the linear system.

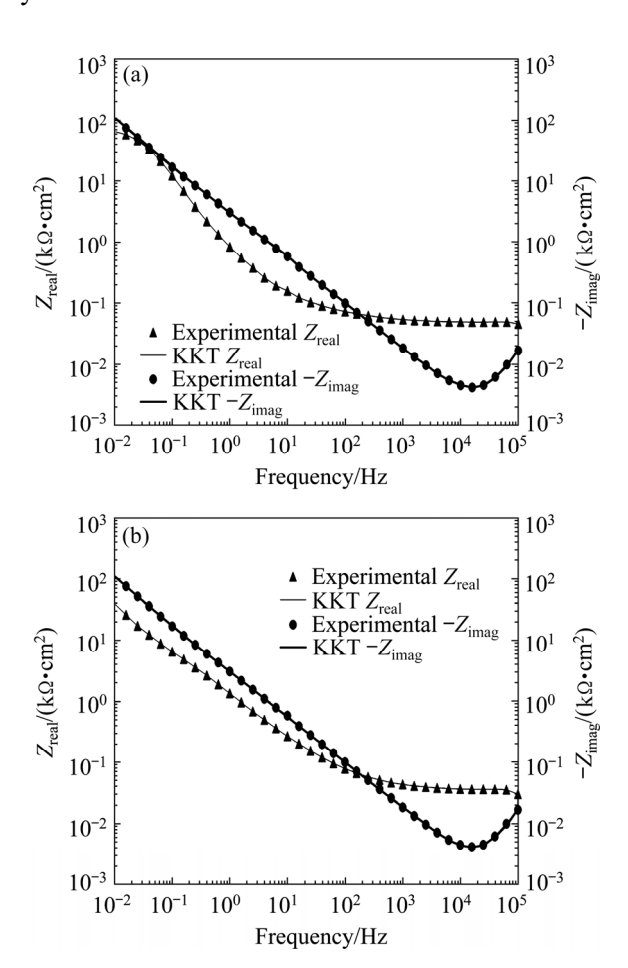


Fig. 6 KKT of EIS results obtained for bare CP-Ti (a) and TB900 (b) samples after 1 h of stabilization in PBS solution with 400 mg/L BSA

It should be mentioned that there may often exist various EECs that represent impedance responses identically; the EIS results were fitted by the most common EEC types for simplicity. Moreover, different formats of the EIS spectra (Fig. 5), the accessible information on EECs used for fitting the EIS curves of the CP-Ti and borided samples in SBF solution [4, 9, 25, 39], and the good quality of fitting according to Chi-square values (χ^2) were considered in the selection of the EEC shown in Fig. 7. As seen, the EIS results of the bare CO-Ti and TB900 samples were fitted by an EEC that included two CPEs. In this EEC, R_s stands for solution resistance; R_2 , R_1 , CPE₂, and CPE₁ denote the resistive contribution of the dense/inner oxide film, the resistive contribution of the porous/outer oxide film, the CPE of the inner film, and the CPE of the outer film, respectively. The impedance of a

CPE (Z_{CPE}) can be expressed as follows [40–42]:

$$Z_{\text{CPE}} = [Q(j\omega)^n]^{-1} \tag{1}$$

where j represents the imaginary unit, ω indexes the angular frequency (rad/s), n marks the deviant degree of a CPE from the ideal capacitance behavior known as the CPE exponent or adjustable parameter, and Q denotes a frequency-independent modulus.

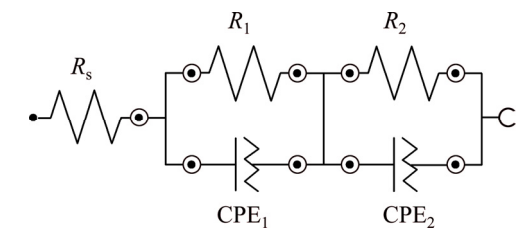


Fig. 7 EEC for simulation of impedance curves of bare CP-Ti and TB900 samples

The obtained values of the fitted EIS spectra are reported in Table 2. Analysis of the parameters in Table 2 revealed that for both the bare CP-Ti and TB900 samples, the resistive contribution of the inner oxide film was remarkably higher than that of the outer one regardless of the immersion time in the studied solution. Hence, the diffusion process occurred in the outer oxide film. In addition, the corresponding resistance of both the inner and outer oxide films showed a general ascending trend with increasing exposure time. On the other hand, a comparison of the polarization resistance (R_p) values for the studied samples at the early stage of immersion illustrated that the R_p of the TB900 sample was remarkably lower than that of the bare CP-Ti sample. This difference was clearly decreased by extending the immersion time. Also, the variation of R_p for the TB900 sample indicates a significant augmentation during the first 24 h (over 29 times). Furthermore, for both studied samples, the CPE exponent values (n) of the inner passive films were relatively high, representing a near capacitance behavior of the surface films developed in the studied solution [43]. Finally, the descending trends of the O values during immersion can be attributed to the thickening of the passive films formed.

According to the mentioned information, the noticeable difference between the R_p values of the two samples (especially early stage during immersion) can be attributed to different surface

Table 2 Electrochemical elements extracted from EIS plots of bare CP-Ti and TB900 samples as function of immersion time in PBS solution containing 400 mg/L BSA

Sample	Immersion time/h	$R_{\rm s}$ / $(\Omega \cdot {\rm cm}^2)$	$R_1/$ $(k\Omega \cdot cm^2)$	$Q_1/$ $(10^{-4} \text{s}^n \cdot \Omega^{-1} \cdot \text{cm}^{-2})$	n_1	$R_2/$ $(k\Omega \cdot cm^2)$	Q_2 / $(10^{-4} s^n \cdot \Omega^{-1} \cdot cm^{-2})$	n_2	$R_{\rm p}/$ $({\rm k}\Omega\cdot{\rm cm}^2)$	χ^2
	1	50.49	7.525	1.45	0.670	1162.300	0.64	0.870	1169.825	5.64×10 ⁻³
Bare	24	50.52	8.251	1.48	0.752	3081.350	0.633	0.920	3089.601	2.05×10^{-3}
CP-Ti	72	48.97	8.882	1.34	0.763	3863.500	0.538	0.930	3872.382	1.63×10^{-3}
	120	48.77	10.077	1.27	0.793	4228.120	0.518	0.940	4238.197	4.25×10^{-3}
TB900	1	46.18	0.036	19.60	0.610	75.960	0.64	0.860	75.996	2.23×10 ⁻³
	24	45.72	0.035	18.78	0.630	2236.740	0.61	0.890	2236.775	2.93×10^{-3}
	72	45.26	0.038	17.67	0.630	3648.130	0.52	0.910	3648.168	6.43×10^{-3}
	120	46.26	0.041	15.89	0.620	3881.240	0.49	0.930	3881.281	6.43×10^{-3}

behaviors of the studied samples for adsorbing PO₄³⁻ and BSA [44]. It seemed that the surface of the bare CP-Ti sample was more capable of forming a protective passive film relative to the TB900 sample in the studied solution under OCP conditions. In contrast, the results of our previous studies [4,9] indicated that the passivation behavior of TB900 was better than that of bare CP-Ti in both Hanks' and Ringer's solutions. These differences could be ascribed to the chemical composition of the studied passive films and solutions.

A passive oxide layer (TiO₂) was formed on the surface of the uncoated CP-Ti specimen. This passive oxide layer adhered to the surface of the specimen; the impermeable and insoluble nature of this layer in aqueous solutions prevented Ti ions from entering the solution [25]. In regard to borided specimen, the boron atoms created defects within the passive layer (TiO₂). Therefore, in the borided specimen, localized sites were available for the passivity breakdown. The electrochemical reactions in the solution containing the borided specimen may lead to the dissolution of the TiB₂ compound and the formation of H₃BO₃ and TiO₂, with the latter being an insoluble compound (see Eqs. (2) and (3)) [9].

$$TiB_2 + 6H_2O \rightarrow Ti^{2+} + 2H_3BO_3 + 3H_2 \uparrow$$
 (2)

$$Ti^{2+} + 2H_2O \rightarrow TiO_2 + 4H^+ + 2e$$
 (3)

3.2.3 M-S analysis results

The M-S assay, which is an in-situ electrochemical technique for evaluating the semiconductive behavior of passive films, was

performed in order to recognize the semiconductor type and determine the charge carrier density variations of the passive films on the studied samples in BSA-containing PBS. According to the point defect model (PDM), the mechanisms of growth, dissolution and breakdown of passive films can be justified by the charge carriers that they contain [45,46]. Therefore, the concentration of these carriers in passive films has been evaluated by many researchers [4,46-49]. Based on the PDM, these charge carriers are classified into two major groups, namely the electron acceptors and the electron donors. It is well known that the electron acceptors are cation vacancies, causing the passive layer to behave as a p-type semiconductor; however, the donors are oxygen vacancies and cation interstitials, resulting in n-type semiconductive properties [46-50]. In the M-S assay, the electrode capacitance (C) is measured as a function of the applied electrode potential (φ) . Under the depletion conditions, there is a linear relationship between the applied potential and the reciprocal of the square of the capacitance (C^{-2}) . The slope of this relationship is used to determine the concentration of the charge carriers [47-52]. The nonlinear behavior in the M-S plot can be ascribed to uniform charge carrier densities [51], the existence of a surface state [52], and surface roughness [53]. For a n-type semiconductor, it can be derived as follows [48–50]:

$$\frac{1}{C^2} = \frac{2}{\varepsilon \varepsilon_0 e N_D} (\varphi - \varphi_{fb} - \frac{K_B T}{e}) \tag{4}$$

where e is the electron charge $(1.60 \times 10^{-19} \text{ C})$, K_{B} stands for the Boltzmann constant $(1.38 \times 10^{-23} \text{ J/K})$,

T indexes the thermodynamic temperature, $\varphi_{\rm fb}$ marks the flat band potential, ε_0 represents the vacuum permittivity (8.854×10⁻¹⁶ F/m), ε stands for the dielectric constant of the passive film, and $N_{\rm D}$ is the acceptor density. The value of the KT/e term is approximately 25 mV at 273 K. The value of the flat band potential can be extracted by extrapolation of the linear region of the M–S curve to C^{-2} =0.

The M-S plots of the bare CP-Ti and TB900 samples obtained after 1 and 120 h of immersion in PBS solution containing 400 mg/L BSA at body temperature are depicted in Fig. 8. As seen, the M-S plots illustrated similar behavior and possess a positive linear region, which implied that the oxide/passive layers formed on the surfaces of the studied samples in PBS acted as n-type semiconductors. In addition, by increasing the immersion time from 1 to 120 h, the positive linear slope of the M-S plots for the samples increased. Therefore, the concentration of the carriers (donors) within the passive films of both samples decreased with increasing exposure time. In other words, the reduction of the carriers occurred, which was

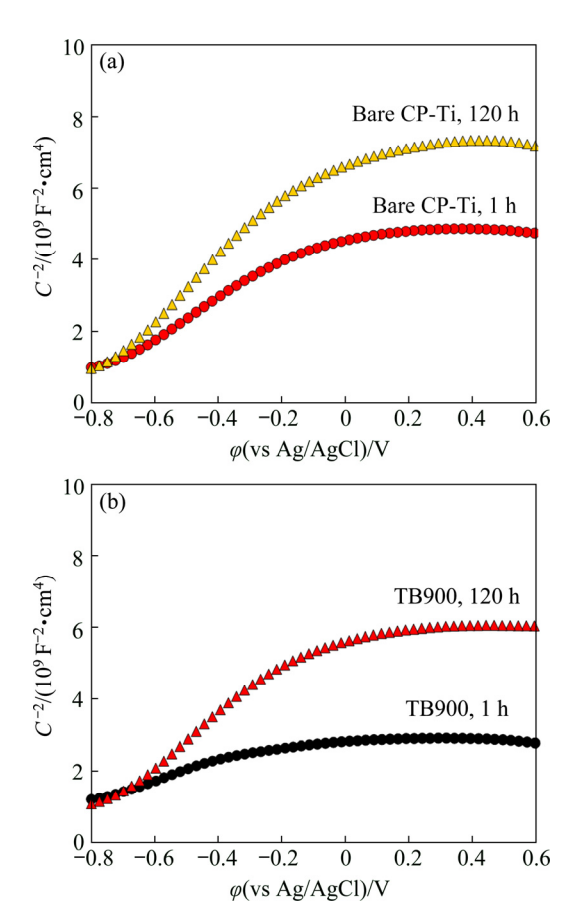


Fig. 8 M–S plots of bare CP-Ti (a) and TB900 (b) samples after 1 and 120 h in PBS solution containing 400 mg/L BSA

indicative of the stability and compaction of the passive films [4,48–50]. Similar behavior was reported for CP-Ti and borided samples in SBF solutions [4,9]. According to Fig. 8, the variations in charge carriers within the passive films of the studied samples in BSA-containing PBS during the studied immersion time were calculated; these results are summarized in Table 3 ($N_{\rm D}(120~{\rm h})/N_{\rm D}(1~{\rm h})$ stands for the donor ratio).

Table 3 Variations in donor concentration of bare CP-Ti and TB900 samples in PBS solution containing 400 mg/L BSA during the first 120 h

Sample	$N_{\rm D}(120 \text{ h})/N_{\rm D}(1 \text{ h})$				
Bare CP-Ti	0.62				
TB900	0.37				

3.2.4 Surface micrographs

The micrographs of the CP-Ti and TB900 samples over 7 d of immersion in PBS solution containing 400 mg/L BSA are shown in Fig. 9. As seen, there were no vestiges of pitting on the specimen surfaces. It seemed that the surface of the TB900 sample was eroded over 7 d of immersion.

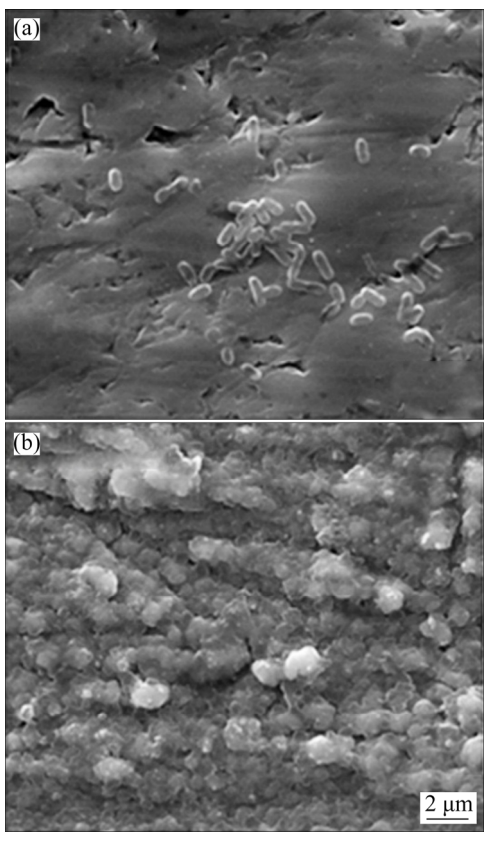


Fig. 9 SEM micrographs of surfaces of CP-Ti (a) and 900TB (b) after 7 d of immersion in BSA-containing PBS solution

3.3 Bioactivity

The regeneration of bone-like apatite on the surface of an implant has an essential role in the process of bone replacement [54]. The morphological changes of CP-Ti and TB900 samples during 21 d of immersion in SBF solution are shown in Fig. 10(a). As observed, the surface morphology of the CP-Ti sample remained constant over the immersion period. In contrast, the borided surface experienced a variety of morphological changes, indicating the effect of the surrounding environment. In addition, the energy-dispersive X-ray spectroscopy (EDS) spectra shown in Fig. 10(b) revealed different chemical natures of the surfaces of the CP-Ti and TB900 samples. As seen, the intensities related to Ca and P were much higher for the TB900 sample relative to the CP-Ti sample, meaning that more bone-like apatite with higher crystallinity deposited on the former. According to the micrographs, it was found that the TiB/TiB₂ coating accelerated the formation of bone-like apatite. The response of the TiB/TiB₂ coating for the formation of bone-like apatite commenced after 14 d of immersion in SBF. Apatite nucleation commenced with the transfer of the PO₄³⁻ and Ca²⁺ from the SBF to the surface, where they bonded with the OH— group of TiOH₄. (TiOH)₄ compound was produced beforehand through the hydrolysis and destruction of the TiO₂ passive film in accordance to Eq. (5) [55]:

$$TiO_2 + 2H_2O = (TiOH)_4$$
 (5)

The electrochemical assays demonstrated the formation of a stable passive film on the TiB/TiB₂ coating, which later acted a facilitator for apatite formation. It should be mentioned that not only the production of Ti—OH groups but also surface charges have significant role in apatite formation.

KAWASHITA et al [56] investigated the role of various metals doped on the CP-Ti surface for apatite-forming ability. They found that apatite formation depended on the chemical states of the doped metals. It seemed that the presence of B on the CP-Ti surface could alter the surface, resulting in greater adsorption of PO₄³⁻ and Ca²⁺ from the SBF to the OH— group of TiOH. Our findings clearly showed that a homogeneous layer of bone-like apatite precipitates covered the TB900 sample surface after 21 d of immersion. These observations confirmed one essential requirement

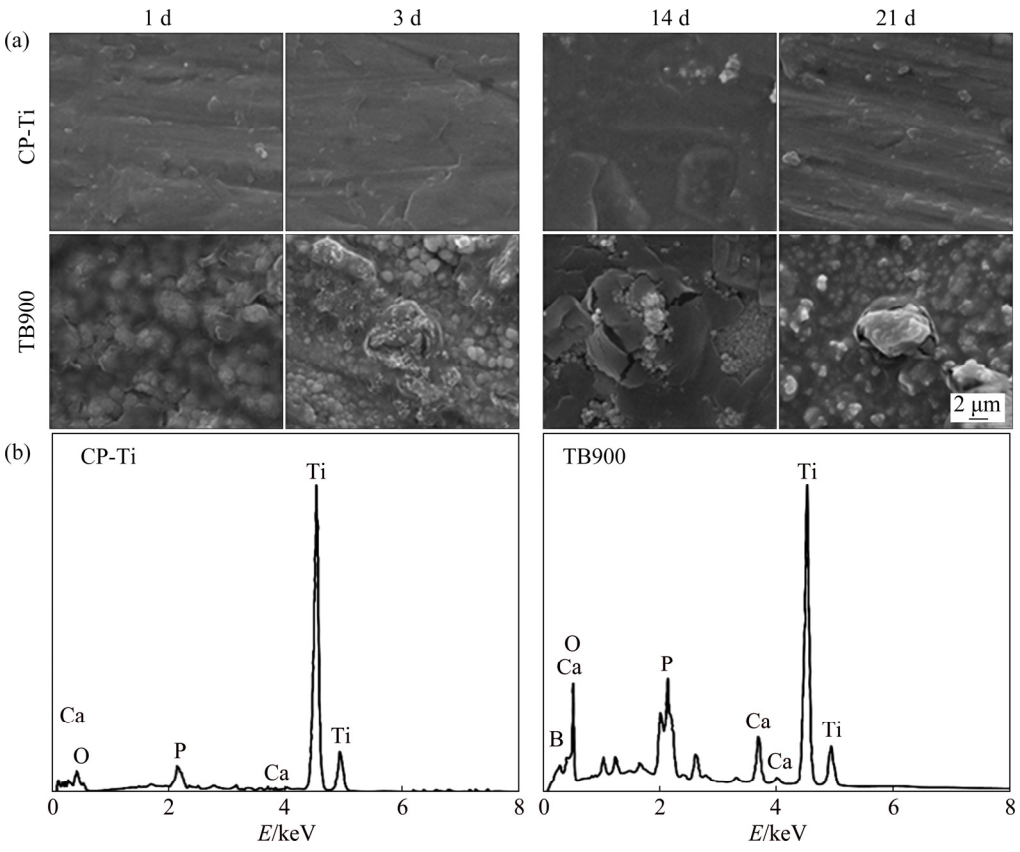


Fig. 10 SEM micrographs of surfaces of CP-Ti and TB900 after 1, 3, 14 and 21 d immersion in SBF (a), and EDS spectra from surfaces of CP-Ti and TB900 over 21 d immersion in SBF (b)

of advanced bioactive materials for bone bonding [57].

3.4 Antibacterial activity

The antibacterial efficiency of pure and borided CP-Ti was studied by evaluating the ability of attached bacteria to form colonies in agar. The attached bacteria are capable of moving and forming more colonies beside the TiB/TiB₂ surface [58]. The assessment of the antibacterial activity showed that CP-Ti had no activity against both E. coli and S. aureus bacteria, with the number of bacteria remaining about 1.4×10³ cfu/mL. In contrast, the results showed that the boriding of CP-Ti caused the destruction of almost all the bacteria across both mentioned species. It is worth mentioning that the number of bacteria remaining beside the borided sample was approximately 10 cfu/mL. On one hand, the OH— group of TiOH, as described in Reaction (5), may degrade the intracellular and extracellular structures bacteria [59,60]. On the other hand, the presence of B atoms on top of the surface enhanced the OH due to the electron deficient nature of B^{3+} [58]. The enhancement of antibacterial activity by boron is not limited to the Ti-B bonds in TiB and TiB2. It has also been found that the Ti-O-B bonds have significant roles in antibacterial activity [58]. Figure 11 displays the photographs of incubated agar plates containing the E. coli and S. aureus bacteria after 24 h against the CP-Ti and TB900 samples. The bacteria growth value was calculated at 40% and -99% with respect to the CP-Ti and TB900 samples, respectively. Our findings are in good agreement with other research on boroncontaining compounds. SOPCHENSKI et al [61] found that the incorporation of B into TiO₂ coatings improved their antibacterial activity, thereby preventing the implant from becoming infected. On the other hand, PRASAD et al [62] found that the presence of B₂O₃ on the surface of an implant enhanced the implant's bioactivity. According to the results, it can be said that the TiB/TiB2 coating had powerful antibacterial activity, making the boriding of Ti a remarkable solution for antibacterial applications. This phenomenon has a great impact on the success of implantation because it can destroy the bacterial biofilm which was formed in peri-implantitis, thereby preventing implant failure [63].

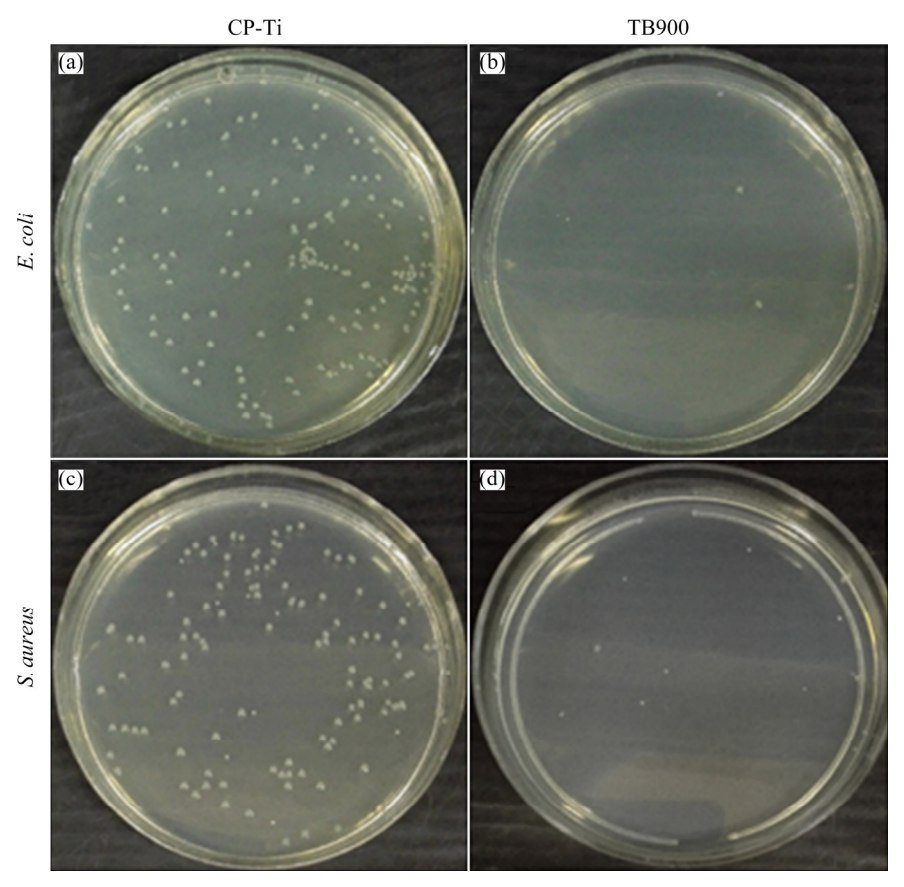


Fig. 11 Photographs showing CP-Ti (a, c) and 900TB (b, d) activity against *E. coli* and *S. aureus* respectively incubated on agar plates for 24 h

Finally, considering the passive film formation on borided CP-Ti in BSA-containing PBS, the generation of bioactive sites, and the excellent antibacterial activity of the TiB/TiB₂ coating, it can be concluded that boriding CP-Ti opens new avenues for more widespread applications of Ti implants.

4 Conclusions

- (1) Characterization of the borided sample by GIXRD demonstrated the formation of the TiB/TiB₂ composite coating on the CP-Ti surface. The wetting ability evaluation showed that boriding of CP-Ti resulted in intermediate water affinity (between hydrophilic and hydrophobic), facilitating greater protein adsorption.
- (2) The electrochemical assays indicated that the corrosion and passive current densities of the bare CP-Ti sample increased through the boriding process. Moreover, M-S measurments indicated that the passive films developed on bare CP-Ti and borided sample had n-type semiconducting behavior.
- (3) The bioactivity evaluation of TiB/TiB_2 coating indicated that the boriding process accelerated bone-like appatite formation on CP-Ti during implanation. The antibacterial activity test against both $E.\ coli$ and $S.\ aureus$ bacteria showed that the CP-Ti had low activity, while the borided CP-Ti destroyed almost all the mentioned bacteria.

Acknowledgments

The authors sincerely acknowledge the Iran National Science Foundation (INSF) for supporting the research under project No. 95841122.

References

- [1] STEVENS M M. Biomaterials for bone tissue engineering [J]. Materials Today, 2008, 11: 18–25.
- [2] ESFAHANI H, DABIR F, TAHERI M, SOHRABI N, TOROGHINEJAD M R. Sol-gel derived hydroxyapatite coating on TiB₂/TiB/Ti substrate [J]. Surface Engineering, 2012, 28(7): 526-531.
- [3] RAMAKRISHNA S, RAMALINGAM M, SAMPATH KUMAR T S, SOBOYEJO W O. Biomaterials: A nano approach [M]. Boca Ration, FL: CRC Press, 2010.
- [4] EBRAHIMI A, ESFAHANI H, FATTAH-ALHOSSEINI A, IMANTALAB O. In-vitro electrochemical study of TiB/TiB₂ composite coating on titanium in Ringer's solution [J]. Journal of Alloys and Compounds, 2018, 765: 826–834.
- [5] MAKUCH N, DZIARSKI P, KULKA M, PIASECKI A,

- TULINSKI M, MAJCORWSKI R. Influence of niobium and molybdenum addition on microstructure and wear behavior of laser-borided layers produced on Nimonic 80A-alloy [J]. Transactions of Nonferrous Metals Society of China, 2019, 29: 322–337.
- [6] KEDDAM M, TAKTAK S. Characterization and diffusion model for the titanium boride layers formed on the Ti6Al4V alloy by plasma paste boriding [J]. Applied Surface Science, 2017, 399(31): 229–236.
- [7] HAI Y Y, WEI Q, CHANG S, GUO P. A first-principle calculation of structural, mechanical and electronic properties of titanium borides [J]. Transactions of Nonferrous Metals Society of China, 2011, 21: 1627–1633.
- [8] SARMA B, TIKEKAR N M, CHANDRAN K S R. Kinetics of growth of superhard boride layers during solid state diffusion of boron into titanium [J]. Ceramics International, 2012, 38: 6795–6805.
- [9] EBRAHIMI A, ESFAHANI H, FATTAH-ALHOSSEINI A, IMANTALAB O. Electrochemical properties of commercially pure Ti with TiB/TiB₂ coatings in Hanks' balanced salt solution [J]. Journal of Materials Engineering and Performance, 2019, 28: 1456–1468.
- [10] SIVAKUMAR B, PATHAK L CHANDRA, SINGH R. Fretting corrosion response of boride coated titanium in Ringer's solution for bio-implant use: Elucidation of degradation mechanism [J]. Tribology International, 2018, 127: 219-230.
- [11] MOHSEN Q, FADL-ALLAH SAHAR A, EI-SHENAWY NAHLA S. Electrochemical impedance spectroscopy study of the adsorption behavior of bovine serum albumin at biomimetic calcium—phosphate coating [J]. International Journal of Electrochemical Science, 2012, 7: 4510–4527.
- [12] DIMAH M K, ALBEZA F D, BORRAS V A, MUNOZ A I. Study of the biotribocorrosion behaviour of titanium biomedical alloys in simulated body fluids by electrochemical techniques [J]. Wear, 2012, 294–295: 409–418.
- [13] KORNYUSHOVA E A, KASHEVSKII A V, ARSENT'EV K Y, PUSHKAREV B G, NIKIFOROV S B, SAFRONOV A Y. Electrochemical behavior of titaniumand platinum in dicarboxilic amino acids solution [J]. Bioelectrochemistry, 2019, 126: 113–120.
- [14] HE X, ZHANG X, WANG X, QIN L. Review of antibacterial activity of titanium-based implants' surfaces fabricated by micro-arc oxidation [J]. Coatings, 2017, 7: 1–24.
- [15] CAMPOCCIA D, MONTANARO L, RENATA C. The significance of infection related to orthopedic devices and issues of antibiotic resistance [J]. Biomaterials, 2006, 27: 2331–2339.
- [16] PATIL D, WASSON M K, ARAVINDAN S, VIVEKANANDAN P, RAO P V. Antibacterial and cytocompatibility study of modified Ti6Al4V surfaces through thermal annealing [J]. Materials Science and Engineering C, 2019, 99: 1007–1020.
- [17] KOKUBO T, TAKADAMA H. How useful is SBF in predicting in vivo bone bioactivity? [J]. Biomaterials, 2006, 27: 2907–2915.
- [18] MURRAY J L, LIAO P K, SPEAR K E. The B-Ti (borontitanium) system [J]. Bulletin of Alloy Phase Diagrams, 1986, 7(6): 550-555.

- [19] MA L S, DUAN Y H, LI P. Microstructure, growth kinetics and some mechanical properties of boride layers produced on pure titanium by molten-salt boriding [J]. Journal of Materials Engineering and Performance, 2017, 26: 4544.
- [20] ZHAO G, XIA L, ZHONG B, WU S, SONG L, WEN G. Effect of alkali treatments on apatite formation of microarc-oxidized coating on titanium alloy surface [J]. Transactions of Nonferrous Metals Society of China, 2015, 25: 1151-1157.
- [21] LU J, YAO C. The role of nanometer and sub-micron surface features on vascular and bone cell adhesion on titanium [J]. Biomaterials, 2008, 29: 970–983.
- [22] SANTOS D, SILVA D M, GOMES P S, FERNANDES M H, SANTOS J D, SENCADAS V. Multifunctional PLLAceramic fiber membranes for bone regeneration applications [J]. Journal of Colloid and Interface Science, 2017, 504: 101–110.
- [23] DAI N, ZHANG L C, ZHANG J, ZHANG X, NI Q, CHEN Y, WU M, YANG C. Distinction in corrosion resistance of selective laser melted Ti-6Al-4V alloy on different planes [J]. Corrosion Science, 2016, 111: 703-710.
- [24] DAI N, ZHANG L C, ZHANG J, CHEN Q, WU M. Corrosion behavior of selective laser melted Ti-6Al-4V alloy in NaCl solution [J]. Corrosion Science, 2016, 102: 484-489.
- [25] SIVAKUMAR B, SINGH R, PATHAK L C. Corrosion behavior of titanium boride composite coating fabricated on commercially pure titanium in Ringer's solution for bioimplant applications [J]. Materials Science and Engineering C, 2015, 48: 243–255.
- [26] BOSE S, PATHAK L C, SINGH R. Response of boride coating on the Ti-6Al-4V alloy to corrosion and fretting corrosion behavior in Ringer's solution for bio-implant application [J]. Applied Surface Science, 2018, 433: 1158-1174.
- [27] SINGH R, MARTIN M, DAHOTRE N. Influence of laser surface modification on corrosion behavior of stainless steel 316L and Ti-6Al-4V in simulated biofluid [J]. Surface Engineering, 2005, 21: 297–306.
- [28] LIAO X, CAO F, ZHENG L, LIU W, CHEN A, ZHANG J, CAO C. Corrosion behaviour of copper under chloridecontaining thin electrolyte layer [J]. Corrosion Science, 2011, 53: 3289–3298.
- [29] MA H, CHEN S, YIN B, ZHAO S, LIU X. Impedance spectroscopic study of corrosion inhibition of copper by surfactants in the acidic solutions [J]. Corrosion Science, 2003, 45: 867–882.
- [30] BAKHSHESHI RAD H R, DAYAGHI E, ISMAIL A F, AZIZ M, AKHAVAN FARID A, CHEN X. Synthesis and in-vitro characterization of biodegradable porous magnesium-based scaffolds containing silver for bone tissue engineering [J]. Transactions of Nonferrous Metals Society of China, 2019, 29: 984–996.
- [31] FATTAH-ALHOSSEINI A, IMANTALAB O, ATTAR-ZADEH F R. Enhancing the Electrochemical behavior of pure copper by cyclic potentiodynamic passivation: A comparison between coarse and nano-grained pure copper [J]. Metallurgical and Materials Transactions B, 2016, 47: 2761–2770.
- [32] LUO H, DONG C, LI X, XIAO K. The electrochemical behaviour of 2205 duplex stainless steel in alkaline solutions

- with different pH in the presence of chloride [J]. Electrochimica Acta, 2012, 64: 211–220.
- [33] LUO H, GAO S, DONG C, LI X. Characterization of electrochemical and passive behaviour of Alloy 59 in acid solution [J]. Electrochimica Acta, 2014, 135: 412–419.
- [34] IZADI M, SHAHRABI T, RAMEZANZADEH B. Active corrosion protection performance of an epoxy coating applied on the mild steel modified with an eco-friendly sol-gel film impregnated with green corrosion inhibitor loaded nanocontainers [J]. Applied Surface Science, 2018, 440: 491-505.
- [35] AKHAVAN H, IZADI M, MOHAMMADI I, SHAHRABI T, RAMEZANZADEH B. The synergistic effect of BTA-Co system on the corrosion inhibition of mild steel in 3.5 wt.% NaCl solution [J]. Journal of the Electrochemical Society, 2018, 165: 670–680.
- [36] BOUKAMP B A. Practical application of the Kramers– Kronig transformation on impedance measurements in solid state electrochemistry [J]. Solid State Ionics, 1993, 62: 131–141.
- [37] SCHÖNLEBER M, KLOTZ D, IVERS-TIFFÉE E. A method for improving the robustness of linear Kramers-Kronig validity tests [J]. Electrochimica Acta, 2014, 131: 20-27.
- [38] FAJARDO S, BASTIDAS D M, CRIADO M, BASTIDAS J M. Electrochemical study on the corrosion behaviour of a new low-nickel stainless steel in carbonated alkaline solution in the presence of chlorides [J]. Electrochimica Acta, 2014, 129: 160-170.
- [39] LIU Y, LIU D, ZHAO Y, CHEN M. Corrosion degradation behavior of Mg-Ca alloy with high Ca content in SBF [J]. Transactions of Nonferrous Metals Society of China, 2015, 25: 3339-3347.
- [40] ESCRIVÀ-CERDÁN C, BLASCO-TAMARIT E, GARCÍA-GARCÍA D M, GARCÍA-ANTÓN J, GUENBOUR A. Effect of potential formation on the electrochemical behaviour of a highly alloyed austenitic stainless steel in contaminated phosphoric acid at different temperatures [J]. Electrochimica Acta, 2012, 80: 248–256.
- [41] HAMADOU L, AÏNOUCHE L, KADRI A, YAHIA S A A, BENBRAHIM N. Electrochemical impedance spectroscopy study of thermally grown oxides exhibiting constant phase element behavior [J]. Electrochimica Acta, 2013, 113: 99–108.
- [42] CHENG X, ROSCOE S G. Corrosion behavior of titanium in the presence of calcium phosphate and serum proteins [J]. Biomaterials, 2005, 26: 7350–7356.
- [43] CHAN C, MAN H, YUE T. Effect of post-weld heat-treatment on the oxide film and corrosion behaviour of laser-welded shape memory NiTi wires [J]. Corrosion Science, 2012, 56: 158–167.
- [44] WANG W, MOHAMMADI F, ALFANTAZI A. Corrosion behaviour of niobium in phosphate buffered saline solutions with different concentrations of bovine serum albumin [J]. Corrosion Science, 2012, 57: 11–21.
- [45] GUPTA R, BIRBILIS N. The influence of nanocrystalline structure and processing route on corrosion of stainless steel: A review [J]. Corrosion Science, 2015, 92: 1–15.
- [46] WANG Q, ZHENG M, ZHU J. Semi-conductive properties of passive films formed on copper in chromate solutions [J]. Thin Solid Films, 2009, 517: 1995–1999.

- [47] WANG L, YU H, WANG S, CHEN B, WANG Y, FAN W, SUN D. Quantitative analysis of local fine structure on diffusion of point defects in passive film on Ti [J]. Electrochimica Acta, 2019, 314: 161–172.
- [48] SELLERS M C, SEEBAUER E G. Measurement method for carrier concentration in TiO₂ via the Mott–Schottky approach [J]. Thin Solid Films, 2011, 519: 2103–2110.
- [49] ROH B, MACDONALD D. Effect of oxygen vacancies in anodic titanium oxide films on the kinetics of the oxygen electrode reaction [J]. Russian Journal of Electrochemistry, 2007, 43: 125–135.
- [50] FATTAH-ALHOSSEINI A, IMANTALAB O, ANSARI G. The role of grain refinement and film formation potential on the electrochemical behavior of commercial pure titanium in Hank's physiological solution [J]. Materials Science and Engineering C, 2017, 71: 827–834.
- [51] SIKORA J, SIKORA E, MACDONALD D D. The electronic structure of the passive film on tungsten [J]. Electrochim Acta, 2000, 45: 1875–1883.
- [52] KONG D S, LU W H, FENG Y Y, YU Z Y, WU J X, FAN W J, LIU H Y. Studying on the point-defect-conductive property of the semiconducting anodic oxide films on titanium [J]. Journal of the Electrochemical Society, 2009, 156: 39–44.
- [53] LI D, WANG J, CHEN D, LIANG P. The role of passive potential in ultrasonic cavitation erosion of titanium in 1 M HCl solution [J]. Ultrasonics Sonochemistry, 2016, 29: 279–287.
- [54] ESFAHANI H, DARVISHGHANBAR M, FARSHID B. Enhanced bone regeneration of zirconia-toughened alumina nanocomposites using PA6/HA nanofiber coating via electrospinning [J]. Journal of Materials Research, 2018, 33(24): 1–9.
- [55] LI B, ZHANG K, YANG W, YIN X, LIU Y. Enhanced corrosion resistance of A/CaTiO₃/TiO₂/PLA coated AZ31 alloy [J]. Journal of the Taiwan Institute of Chemical Engineers, 2016, 59: 465–473.

- [56] KAWASHITA M, IWABUCHI Y, SUZUKI K, FURUYA M, YOKOTA K, KANETAK H. Surface structure and in vitro apatite-forming ability of titanium doped with various metals [J]. Colloid and Surface A, 2018, 555: 558–564.
- [57] KOKUBO T, YAMAGUCHI S. Simulated body fluid and the novel bioactive materials derived from it [J]. Journal of Biomedical Materials Research: Part A, 2019, 107(5): 968–977.
- [58] WANG Y, XUE X, YANG H. Synthesis and antimicrobial activity of boron-doped titania nano-materials [J]. Chinese Journal of Chemical Engineering, 2014, 22(4): 474–479.
- [59] WANG G, FU H, ZHAO Y, ZHOU K, ZHU S. Bone integration properties of antibacterial biomimetic porous titanium implants [J]. Transactions of Nonferrous Metals Society of China, 2017, 27: 2007–2014.
- [60] CHEN M, LI H, WANG X, QIN G, ZHANG E. Improvement in antibacterial properties and cytocompatibility of titanium by fluorine and oxygen dual plasma-based surface modification [J]. Applied Surface Science, 2019, 463: 261–274.
- [61] SOPCHENSKI L, COGO S, DIAS-NTIPANYJ M F, ELIFIO-ESPÓSITO S, POPAT K C, SOARES P. Bioactive and antibacterial boron doped TiO₂ coating obtained by PEO [J]. Applied Surface Science, 2018, 458: 49–58.
- [62] PRASAD S S, DATTA S, ADARSH T, DIWAN P, ANNAPURNA K, KUNDU B, BISWAS K. Effect of boron oxide addition on structural, thermal, in vitro bioactivity and antibacterial properties of bioactive glasses in the base S53P4 composition [J]. Journal of Non-Crystalline Solids, 2018, 498: 204–215.
- [63] BESINIS A, HADI S D, LE H R, TREDWIN C, HANDY R D. Antibacterial properties of silver nanoparticles grown in situ and anchored to titanium dioxide nanotubes on titanium implant against *Staphylococcus aureus* [J]. Nanotoxicology, 2017, 11(3): 327–338.

含 BSA 的 PBS 中硼化工业纯钛的 生物活性、抗菌活性和电化学行为

Adib EBRAHIMI, Hamid ESFAHANI, Omid IMANTALAB, Arash FATTAH-ALHOSSEINI

Department of Materials Engineering, Bu-Ali Sina University, Hamedan 65178-38695, Iran

摘 要:研究硼化物涂层对含牛血清白蛋白(BSA)的磷酸盐缓冲液(PBS)中工业纯钛(CP-Ti)的生物活性、抗菌活性和电化学行为的影响。掠入射 X 射线衍射(GIXRD)谱证实,经硼化处理已形成 TiB/TiB₂涂层。扫描电镜(SEM)测试表明,TiB₂交联颗粒覆盖 TiB 晶须。水接触角测量发现,硼化处理导致形成具有中间亲水性的表面。动电位极化(PDP)测试表明,在含 BSA 的 PBS 中 TiB/TiB₂涂层具有可接受的钝化行为。电化学阻抗谱(EIS)测量表明,延长暴露时间使 CP-Ti 和硼化样品的钝化行为得到改善。根据 Mott-Schottky (M-S)分析结果,两种样品钝化膜的载流子均随样品在含 BSA 的 PBS 中暴露时间的延长而减少。模拟体液中的生物活性测试表明,TiB/TiB₂涂层使CP-Ti 从生物惰性材料转变成生物活性材料。最后,对大肠杆菌和金黄色葡萄球菌的抗菌活性测试表明,TiB/TiB₂涂层的抗菌活性为99%。

关键词: 电化学行为; 硼化; 含牛血清蛋白(BSA)的磷酸盐缓冲液(PBS); 钝化膜; 硼化钛